AFRL-RX-WP-TR-2022-0147

ACOUSTICALLY PUMPED ON-CHIP OPTICAL ISOLATORS

Gaurav Bahl
University of Illinois

26 JUNE 2022
Final Report

AIR FORCE RESEARCH LABORATORY
MATERIALS AND MANUFACTURING DIRECTORATE
WRIGHT-PATTERSON AIR FORCE BASE, OH 45433-7750
AIR FORCE MATERIEL COMMAND
UNITED STATES AIR FORCE

NOTICE AND SIGNATURE PAGE

Using Government drawings, specifications, or other data included in this document for any purpose other than Government procurement does not in any way obligate the U.S. Government. The fact that the Government formulated or supplied the drawings, specifications, or other data does not license the holder or any other person or corporation; or convey any rights or permission to manufacture, use, or sell any patented invention that may relate to them.

Qualified requestors may obtain copies of this report from the Defense Technical Information Center (DTIC) (http://www.dtic.mil).

AFRL-RX-WP-TR-2022-0147 HAS BEEN REVIEWED AND IS APPROVED FOR PUBLICATION IN ACCORDANCE WITH ASSIGNED DISTRIBUTION STATEMENT.

GRIFFIN.BENJAMIN.GEORGE.1473615351 Digitally signed by GRIFFIN.BENJAMIN.GEORGE.1473615351 Date: 2022.10.19 13:07:50 -04'00'

BENJAMIN GRIFFIN
Program Manager
Electronic Materials Branch
Photonic, Electronic, and Soft Matter
Materials Division
Materials and Manufacturing Directorate

SCHMITT.MARK.G.1257789701 Digitally signed by SCHMITT.MARK.G.1257789701 Date: 2022.10.19 15:02:56 -04'00'

MARK SCHMITT
Branch Chief
Electronic Materials Branch
Photonic, Electronic, and Soft Matter
Materials Division
Materials and Manufacturing Directorate

This report is published in the interest of scientific and technical information exchange, and its publication does not constitute the Government's approval or disapproval of its ideas or findings.

REPORT DOCUMENTATION PAGE

Form Approved
OMB No. 0704-0188

1. REPORT DATE *(DD-MM-YY)*	2. REPORT TYPE	3. DATES COVERED *(From - To)*
26 June 2022	FINAL	28 August 2019 – 26 August 2022

4. TITLE AND SUBTITLE
Acoustically Pumped On-Chip Optical Isolators

5a. CONTRACT NUMBER
FA8650-19-2-7924

5b. GRANT NUMBER

5c. PROGRAM ELEMENT NUMBER
DARPA

6. AUTHOR(S)
Gaurav Bahl

5d. PROJECT NUMBER

5e. TASK NUMBER

5f. WORK UNIT NUMBER
X1R1

7. PERFORMING ORGANIZATION NAME(S) AND ADDRESS(ES)
Board of Trustees of the University of Illinois
352 Henry Administration Building
506 S. Wright Street
Urbana, IL 61801

8. PERFORMING ORGANIZATION REPORT NUMBER

9. SPONSORING/MONITORING AGENCY NAME(S) AND ADDRESS(ES)
Air Force Research Laboratory
Materials and Manufacturing Directorate
Wright-Patterson Air Force Base, OH
45433-7750
Air Force Materiel Command
United States Air Force

10. SPONSORING/MONITORING AGENCY ACRONYM(S)
AFRL/RXAN

11. SPONSORING/MONITORING AGENCY REPORT NUMBER(S)
AFRL-RX-WP-TR-2022-0147

12. DISTRIBUTION/AVAILABILITY STATEMENT
DISTRIBUTION STATEMENT A. Approved for public release; distribution is unlimited.

13. SUPPLEMENTARY NOTES
Report contains color.

14. ABSTRACT

The primary goal of this fundamental research project was to demonstrate magnet-free on-chip optical isolators, especially near 780 nm wavelength, as these can be important device components in future microsystems based on atomic microsystems technologies. We were successful in developing this new optical isolator using a lithium niobate PIC platform. Instead of magneto-optic materials, this isolator uses an electrical stimulus to piezoelectrically launch acoustic waves through the PIC and produce a non-reciprocal effect. The isolators were proven to operate at both 780 nm and 1550 nm using the same starting substrate, successfully reaching the project goals.

15. SUBJECT TERMS
Optical Isolators, Integrated Photonics, Non-reciprocal Devices, Lithium Niobate, Atomic Microsystems

16. SECURITY CLASSIFICATION OF:			17. LIMITATION OF ABSTRACT:	18. NUMBER OF PAGES	19a. NAME OF RESPONSIBLE PERSON (Monitor)
a. REPORT	b. ABSTRACT	c. THIS PAGE			Benjamin Griffin
Unclassified	Unclassified	Unclassified	SAR	21	19b. TELEPHONE NUMBER *(Include Area Code)* (937) 255-9904

Table of Contents

Section **Page**

List of Figures

Figure **Page**

1. Summary

The primary goal of this fundamental research project was to demonstrate magnet-free on-chip optical isolators, especially near 780 nm wavelength, as these can be important device components in future microsystems based on atomic microsystems technologies. The isolator needed to exhibit extremely low insertion loss with very high directional contrast, and we needed to show a path towards photonic integration in a foundry-like process without the use of any magnetic materials.

In the past few decades, tremendous progress has been made towards producing chip-scale photonic integrated circuits (PICs) for sensing and communications, in both civilian and defense applications. In this context, optical isolators are critical non-reciprocal devices that can protect laser sources and can additionally ensure robust operation of such photonic systems. As their function is to only allow unidirectional transmission of light, isolators are conventionally produced using materials that exhibit a strong magneto-optic effect. Unfortunately, current magneto-optic isolator architectures cannot be scaled and translated into common PIC platforms due to multiple technical constraints. The magneto-optic approach is especially unsuitable for quantum sensing applications and for interfacing photons with atomic systems, as the magnetic fields can produce adverse effects. A generalized non-reciprocal photonic component technology that avoids these constraints would be a transformative development.

Our technical solution utilized direction-selective interference of optical modes in a multi-resonant device, generated by non-reciprocal inter-band scattering of light from phonons (acoustic waves). In principle, the isolator device we demonstrated can be lossless for light propagating in one direction and strongly absorbing in the opposite direction, i.e. it can exhibit complete linear optical isolation. Moreover, the demonstrated devices do not require any magneto-optic materials and could enable production of optical isolators over a variety of optical wavelengths.

We were successful in developing this new optical isolator using a lithium niobate PIC platform that we developed at the University of Illinois that can be easily ported to foundries [1]. Instead of magneto-optic materials, this isolator uses an electrical stimulus to piezoelectrically launch acoustic waves through the PIC and produce a non-reciprocal effect [2]. As the main result from this effort, we demonstrated optical isolators with < 1 dB forward loss and > 39 dB directional contrast. The isolators were proven to operate at both 780 nm and 1550 nm using the same starting substrate, successfully reaching the project goals.

2. Introduction

An optical isolator is a two-port optical device that only allows light to pass through one way, but blocks transmission in the opposite direction. Such non-reciprocal behavior is not achievable without either breaking time-reversal symmetry or using non-linearity within the material. The typical commercial approach for producing isolators is to use the magneto-optic effect, but this mechanism is not suitable in many scenarios that are of contemporary interest. The central technical challenge motivating our effort was a desperate need for on-chip integrated isolators that can resolve the following list of technical problems –

(1) Magnets and magneto-optic materials cannot be readily integrated on-chip and are not available in commercial foundries,
(2) The optical attenuation associated with available magneto-optic materials are quite large and result in lossy devices,
(3) Magneto-optic coefficients are quite small for currently available materials and each design for a desired operational wavelength needs a custom material and custom biasing,
(4) Zeeman shifts associated with magneto-optic isolators are undesirable in cold-atom microsystems technologies, and
(5) Magneto-optic isolators are not usually dynamically reconfigurable.

Due to the above technical limitations, extensive research has been conducted by many groups on alternative isolator technologies. Many of these past approaches operate over a narrow bandwidth, which is acceptable for many applications like ultra-stable laser sources, LIDAR, and atomic referencing. While several of these alternatives have proven good optical contrast for isolation, the ability to provide low insertion loss has remained a significant technical challenge.

3. Methods, Assumptions, and Procedures

3.1. Our guiding concept for developing an ideal isolator on chip

The ideal two-port nearly-lossless device is simply a high-quality linear waveguide of short length, and would represent the best case for the lowest forward loss in the `high transparency' direction of an isolator. To this waveguide we now introduce an absorbing component, e.g. a high-Q resonator that operated over a narrow bandwidth, that is coupled to this waveguide in shunt configuration. If the absorber is frequency-detuned by a few linewidths from the frequency of interest, a high transparency is observed in the waveguide since the absorber will not be accessible. As the opposite case, if the light in the waveguide is on resonance with the absorber, and if the absorber is additionally critically coupled, then a very large attenuation factor is achieved. Our guiding concept behind the isolator device is that this near-ideal transparency and giant attenuation can be simultaneously exploited using a narrow-band absorber with specific chiral properties (see Fig 1). A key component of our project was therefore to demonstrate this chiral absorption effect within a whispering-gallery or racetrack resonator.

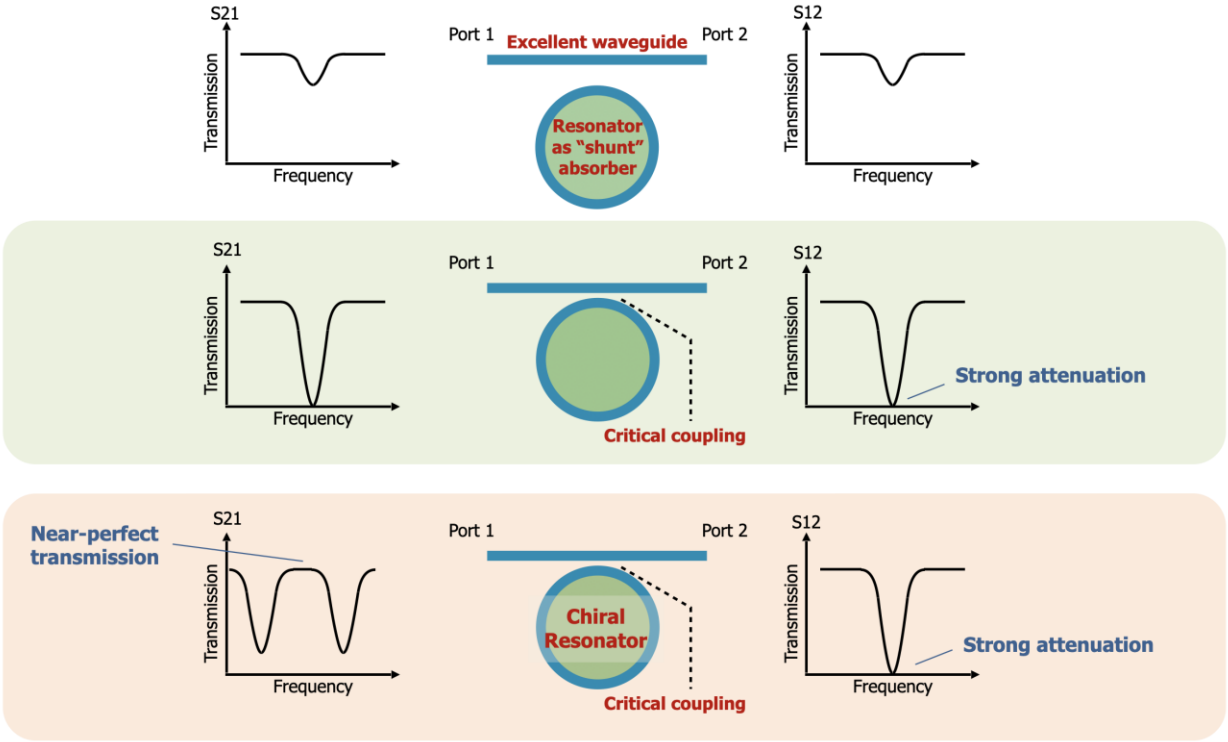

Figure 1. Visualization of the non-reciprocal shunting approach to producing near-ideal optical isolators. (Top) The interaction of a whispering-gallery (or racetrack) resonator with a waveguide can be optimized (see Middle) to produce strong attenuation, i.e. light-blocking behavior. (Bottom) If this resonator has chiral dispersion, then near-ideal isolator characteristics can be produced.

3.2. Preliminary work

In preliminary research, we had implemented an electrically-driven non-reciprocal (or chiral) nanophotonic modulator near 1550 nm [2] using an aluminum nitride (AlN) on insulator photonic platform. The device was composed of a waveguide coupled to a racetrack resonator in an architecture similar to Fig 1. Light propagating through the waveguide from one direction is scattered to a different optical mode through phonon-mediated momentum shift and energy shift, known as indirect inter-band (or inter-modal) scattering. Light propagating the opposite direction does not experience the inter-band coupling and is simply resonantly absorbed. The requisite effect is produced using a piezoelectric actuator with radiofrequency drive stimulus, and the non-reciprocal behavior can therefore be dynamically adjusted. Further details on this symmetry breaking mechanism can be found in our paper [2].

A nonreciprocal modulator, as described here, already provides the functional capability of optical isolation, albeit with a known frequency shift of the light in the forward direction. Thus, one path would be to proceed with a 780 nm implementation of the same result. However, it is not practical to obtain ultra-low loss isolation through this approach due to losses inherent in mode-conversion. As a result, our goal on this project was to use the same structure of modes as described above, but to push the system into the "strong coupling regime" where the system exhibits a linear (not frequency shifting) isolator behavior. Through this innovative approach in which mode-conversion is avoided, the forward insertion loss can be brought to near zero.

3.3. Isolator operating principle (photonic Autler-Townes splitting)

To produce our isolator, we again used a racetrack resonator supporting two circulating optical modes at distinct frequency and momentum. A piezoelectric surface acoustic transducer was fabricated to act as a "phonon pump" that breaks orthogonality of the optical modes through acousto-optic scattering. As shown in the phase-matching diagram in Fig 2, the acousto-optic coupling is only engaged for clockwise circulating (forward propagating from the waveguide perspective, from port 1 to port 2) optical signals. For light propagating in the opposite direction (in the waveguide from port 2 to port 1), the momentum difference between the optical modes is not satisfied by these driven phonons. Thus, the system exhibits broken symmetry, i.e. inter-modal coupling is permitted only in the forward direction while the backward signals see no such effect.

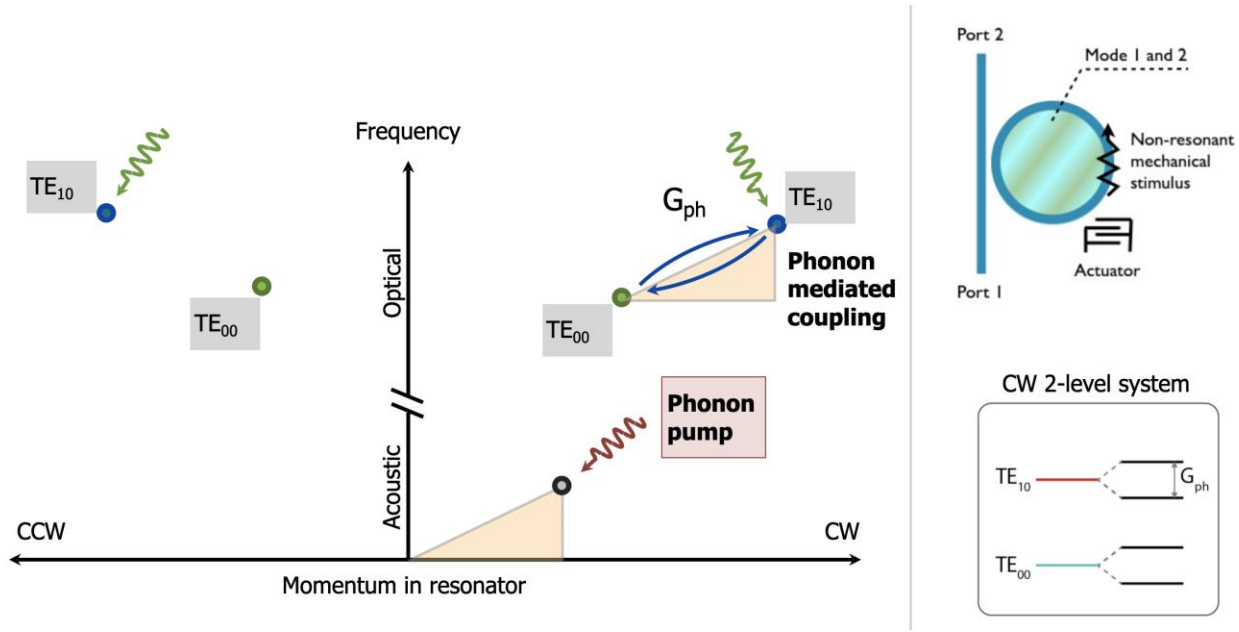

Figure 2. Phase-matching diagram for non-reciprocal intermodal scattering within a ring resonator that is used to produce optical isolation. The available optical modes of the resonator can be treated as two independent two-level "photonic atoms" in either cw or ccw directions. Using unidirectional piezoelectrically actuated phonons, the coupling between only one set (e.g. clockwise, cw) of optical levels is engaged. This system is not symmetric under time-reversal since there is no optomechanical phase-matching in the ccw direction and therefore light propagating in the reverse direction is resonantly absorbed. (Bottom-right inset) When the optomechanical coupling rate G_{ph} becomes sufficiently large, the photonic atom in the cw direction exhibits a process similar to Autler-Townes splitting, which prevents light absorption.

In both clockwise and counterclockwise directions, the system can be treated as two independent two-level "photonic atoms". Presently, we consider only the clockwise direction where phase-matching is satisfied. When the optomechanical coupling rate G_{ph} exceeds the individual optical mode linewidths (e.g. for large piezoelectric drive power), we enter the strong coupling regime in which the two optical modes hybridize and exhibit normal mode splitting (equivalent to Autler-Townes splitting or ATS) as shown in Fig 2 (bottom-right). This "photonic ATS" process causes the optical density of states to split into two "dressed states" in the clockwise direction (see Fig 3), allowing light to pass through the waveguide without interacting with the resonator. In this strong coupling condition, as shown in Fig 3, at the zero detuning point the transmission loss approaches zero in one direction only.

This strong coupling regime can be reached with very large opto-acoustic coupling rates and with the use of high Q-factor modes. Therefore, improvements to the piezo-transducer and to the mechanical and optical resonances were important. This is main reason why we developed our isolator in lithium niobate (as described below), although in principle there is no material restriction provided the strong coupling regime can be reached. Formally, the strong coupling or photonic ATS regime transition occurs when the optomechanical coupling rate exceeds a critical value $G_{ph,crit} = \sqrt{\kappa_1 \kappa_2}/2$ where κ_i are the optical loss rates of the individual modes.

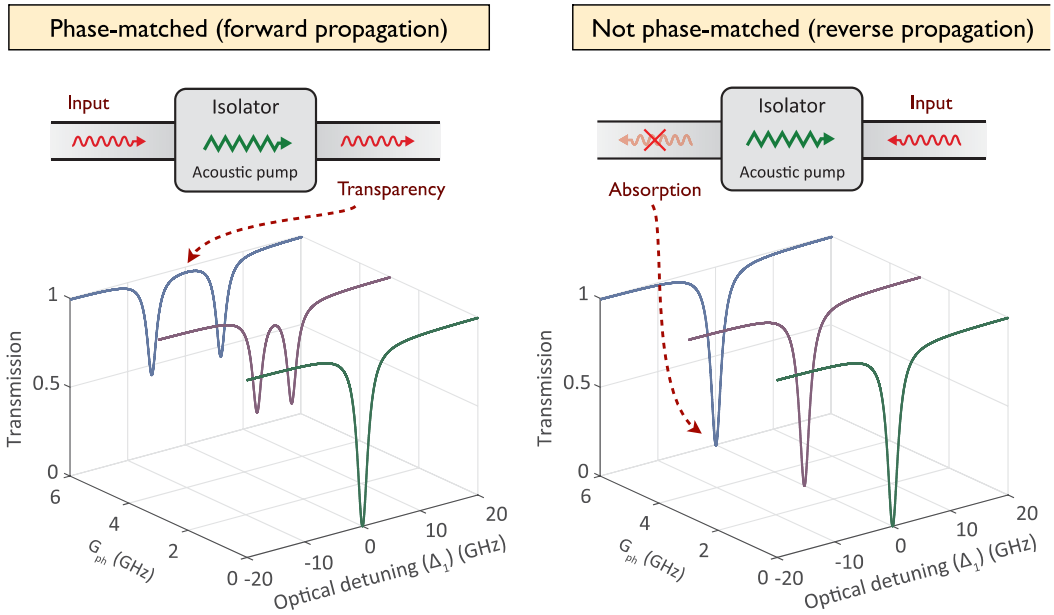

Figure 3. As the optomechanical coupling rate G_{ph} increases (higher radiofrequency electrical input to the piezoelectric actuator leading to higher phonon stimulus), the photonic ATS process results in improved optical transparency in the phase-matched direction only. In the strong coupling regime, the transmission can approach 100% at zero detuning in one direction while the opposite direction remains absorbing. The absorbing direction can be optimized into "critical coupling".

4. Results and Discussion

4.1. Isolator fabrication and experimental results

We developed an integrated photonics platform based on lithium niobate-on-insulator (LNOI) technology – shown in Fig 4. Fabrication of both of our isolator demonstrations (at 1550 nm and 780 nm) begins with an LNOI wafer that is commercially purchased with 500 nm thickness X-cut LN device layer, 2 μm buried oxide, and high resistivity silicon substrate. The resonators, waveguides, and grating couplers were all patterned using electron-beam lithography. The LN layer was then partially etched using argon-based ICP-RIE physical etching. The resulting cross-section is of ridge geometry (Fig. 4). For the 780 nm isolator, we initially reduced the device layer thickness to 300 nm prior to further patterning. This ensures single-mode operation of the waveguide and two-mode operation of the racetrack resonator. As a point of flexibility, this thickness may be varied locally to accommodate other desired wavelengths for the isolator operation. To achieve radiofrequency (RF) excitation of the acoustic waves, we patterned an aluminum interdigitated transducer (IDT) oriented at 30^{o} from +y axis of the LN to ensure the best electromechanical coupling. All design parameters are discussed in detail in our published journal paper and its supplement [1].

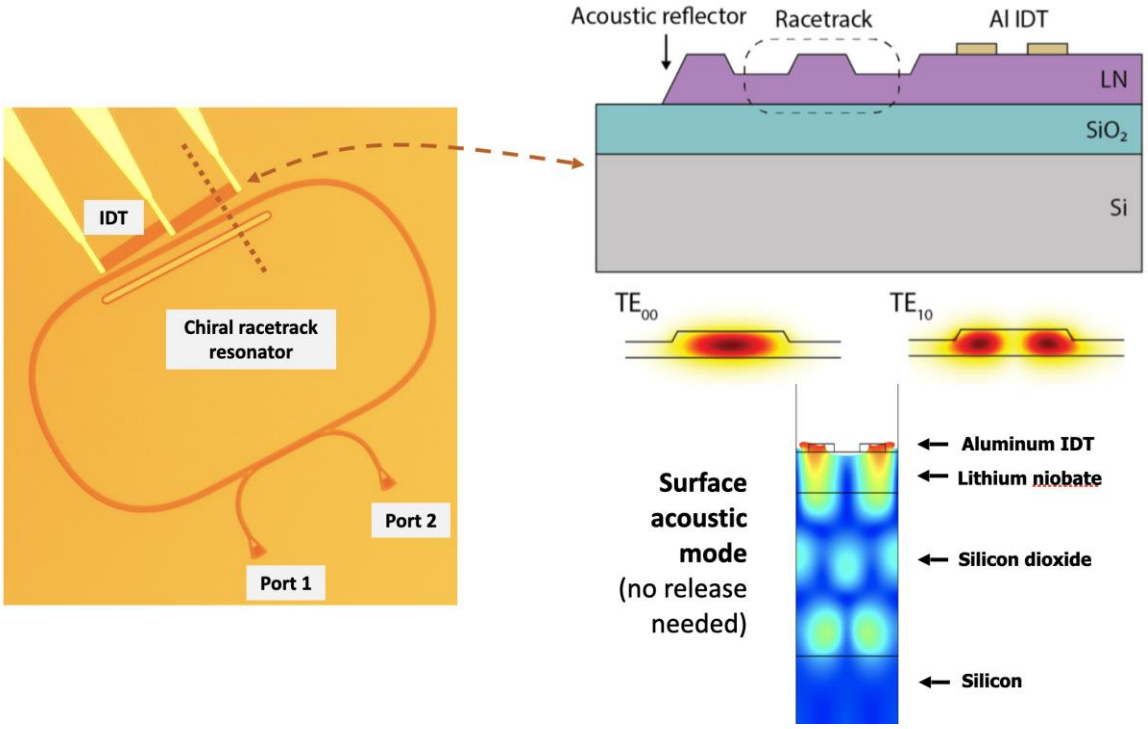

Figure 4. (Left) Microscope view of the entire optical lithium niobate isolator device, showing the racetrack resonator, metal interdigital transducer (IDT) electrodes, acoustic reflector, and input/output grating couplers forming the optical ports. (Top-right) The device cross-section is shown here, along with simulations of the key optical modes participating in the design. (Bottom-right) This cross-section shows a real-scale simulation of the surface acoustic wave that is excited in the lithium niobate layer by radiofrequency (RF) stimulation of the aluminum IDT.

The optical advantage of single-crystal lithium niobate (LN) is its wide bandgap that provides a transparency window spanning 350 nm to 5300 nm. The high piezoelectric coefficients of LN also permit efficient actuation of surface acoustic waves via RF stimulus electrodes. In comparison, our previous efforts used aluminum nitride (AlN) as the photonic and piezoelectric material [2], [3]. With LN we were able achieve much higher optical Q-factors for racetrack resonators (10^7 at 780 nm, $3.5x10^6$ at 1550 nm) and ~10x higher electromechanical transduction efficiency than AlN. Example of our highest measured Q-factor resonators are presented in Fig 5.

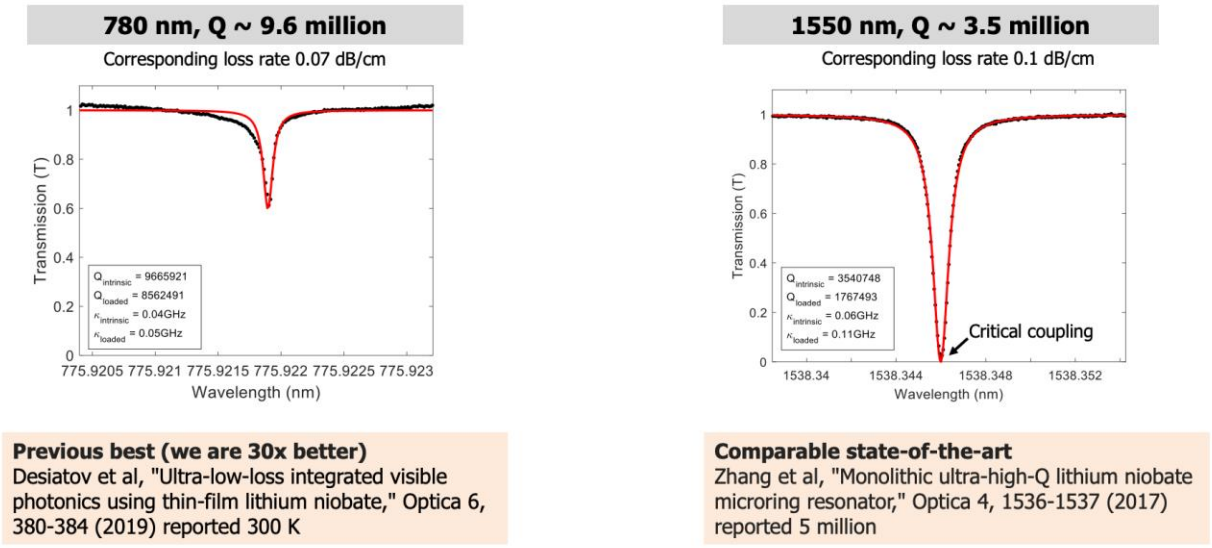

Figure 5. (Left) Our best measured optical Q-factors near 780 nm. (Right) Our best measured optical Q-factor near 1550 nm. We also provide comparisons to the best contemporary results.

A representative series of experimental measurements is presented in Fig 6. Details on the experimental setup used to acquire these measurements are presented in our paper [1]. We find that the device behavior is as expected – as we increase the RF stimulus power, the TE_{00} and TE_{10} modes inside the resonator hybridize into a pair of dressed states due to the photonic ATS effect. This results in a high transparency only for the direction in which the process is phase-matched (here it is 1->2), while at the same time there is no significant change in the opposite direction (from 2->1). We can compare both forward and backward transmission measurements on a single plot to see the isolator operation. We present our best measurements at both 1550 and 780 nm in Fig 7. The key regions of interest are highlighted on the plot along with quantifications of the important parameters at the center of the effect.

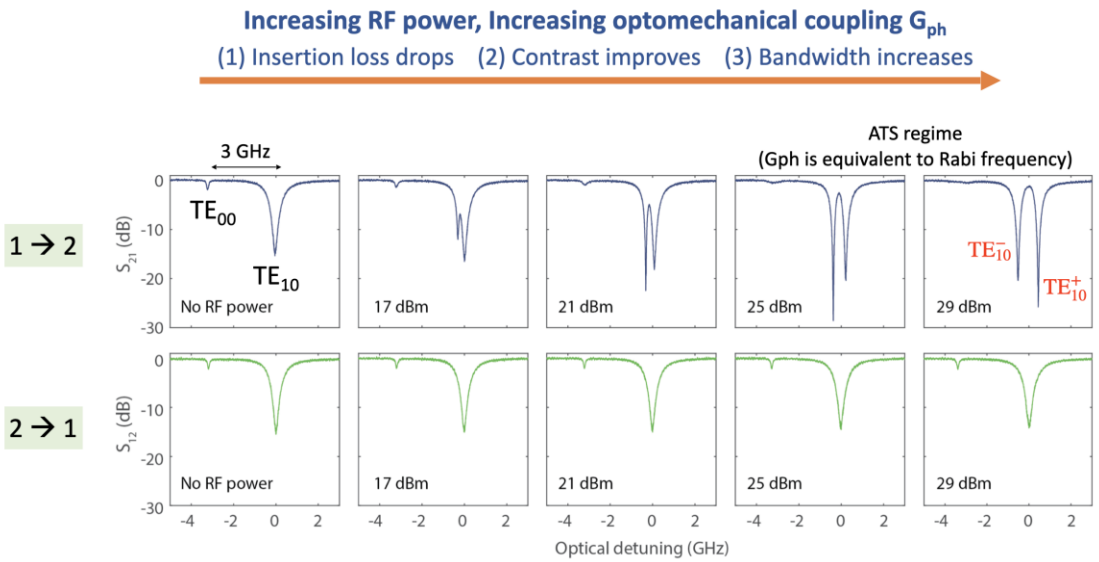

Figure 6. These experimental results showcase the optical transmission through the waveguide in both forward (1->2) and backward (2->1) through the optical grating couplers for evolving RF stimulus power up to 29 dBm. The transmission is normalized by setting the baseline to 0 dB and therefore factors out any losses incurred at the grating couplers.

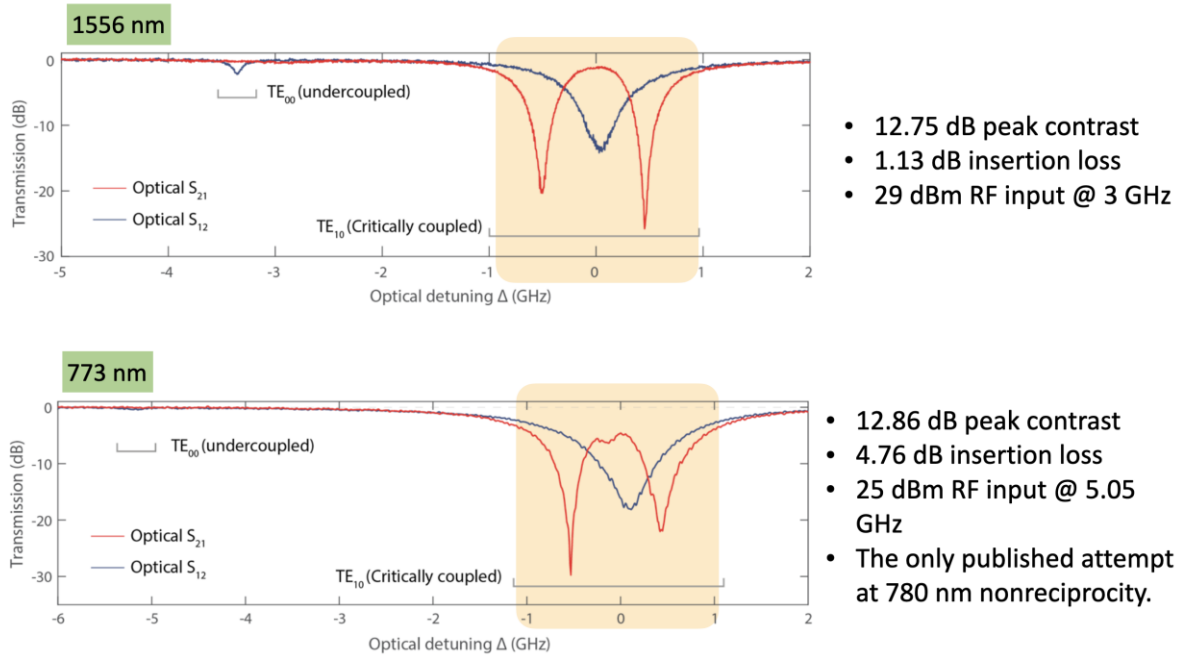

Figure 7. (Top) Our best measured isolator device operating near 1550 nm. The transmission loss is very small ~1.13 dB around the middle of the effect (red trace) while the light is blocked in the opposite direction (blue trace). We note here that these quantifications are made at the central point of the effect and signal bandwidths must also be considered. (Bottom) Similarly, we showcase our best isolator device at 780 nm. It is important to emphasize that there is no past work on on-chip isolators near 780 nm. These figures are adapted from our journal paper [1].

We find from the above experimental results that both types of devices provide clear experimental evidence of the desired mode of operation. Further optimizations could be performed to improve the level of G_{ph} and the Q-factors of the optical modes. Various alternative architectures can also be envisioned as future work in which the Q-factor is traded for additional bandwidth.

4.2 Demonstration of a surprising non-reciprocal effect that outperforms the initial concept

In the above photonic ATS-based approach, the non-reciprocity is strongly dependent on the fabricated geometry since that determines the criticality of coupling between the waveguide and the primary optical mode (i.e. which determines attenuation in the non-phase matched direction). A solution for better control of contrast is to instead leverage the dressed states, i.e. the nonreciprocal wings to either side of the transparency central band. In these adjacent frequency ranges the definition of forward and backward transmission should be reversed. The contrast here is dictated by coupling to the dressed states and is therefore a function of G_{ph}, and of the relative mismatch between the optical mode separation and the applied acoustic/RF frequency. We were able to show that if the primary optical mode is over-coupled then there exists a choice of G_{ph} and modal mismatch where critical coupling is achievable on a dressed state. Our best example of this case is shown in Fig. 8, where on the lower dressed state we measured ~0.65 dB insertion loss with ~39 dB contrast. We also implemented this effect with a device operating near 780 nm (presented in the supplement of our manuscript [1]). We believe that this is the best mode of operation for future versions of these isolators as it could be tuned using the input degrees of freedom (e.g. RF power, frequency, etc), even after the device is fabricated and packaged.

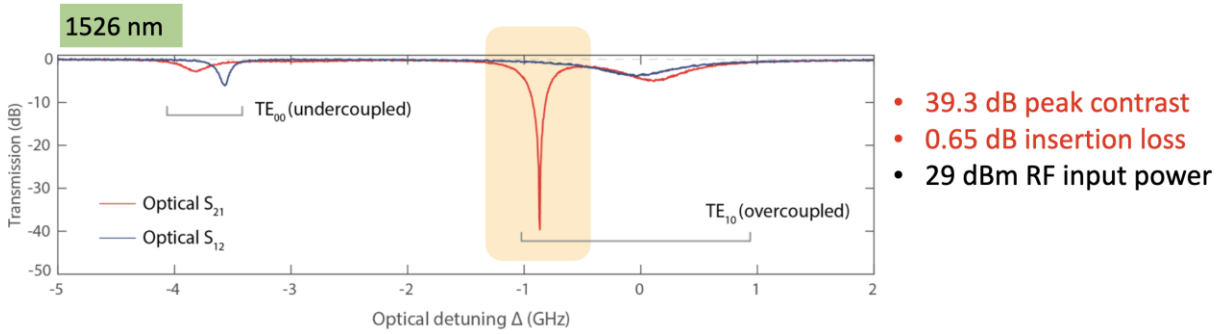

Figure 8. A new and much stronger non-reciprocal effect can be generated by optimizing coupling to the dressed states of the hybrid opto-mechanical system. Here were observe record-breaking figure of merit of 60 dB/dB IC/IL (described below). Figure is adapted from our paper [1].

4.3. Comparison to alternative approaches

In the Supplementary Information accompanying our publication [1] we presented a detailed comparison to other monolithically integrated, linear response optical isolators (reproduced below in Fig 9). We found that magneto-optic isolators did consistently exhibit higher bandwidth than both electro-optic and acousto-optic alternatives. On the other hand, non-resonant isolators (e.g.

waveguide-based isolators) also have a bandwidth advantage but are generally inefficient in terms of power requirements and exhibit high insertion loss.

Since isolators can be cascaded, the best figure of merit (FoM) is the ratio of isolation contrast (IC in dB) per forward insertion loss (IL in dB). On this figure of merit, our best demonstration device exhibited contrast at par with magneto-optic isolators but outperformed them by having the lowest insertion loss of all previous demonstrations, and also set an optical isolator figure of merit record at 60 dB/dB IC/ IL.

Author	Year	Device Type	Technique	Peak isolation contrast (IC)	Insertion loss (IL)	Peak IC per 1 dB IL (dB/dB)	10 dB IC Bandwidth	20 dB IC Bandwidth	Wavelength
This work	-	Resonator	AO	39.31 dB	0.65 dB	60.46	108.8 MHz	33.1 MHz	1550 nm
This work	-	Resonator	AO	12.75 dB	1.13 dB	11.28	198.5 MHz	N/A	1550 nm
This work	-	Resonator	AO	12.86 dB	4.76 dB	2.7	202 MHz	N/A	780 nm
Kim et. al. [S10]	2021	Resonator	AO	3 dB	9 dB	0.33	N/A	N/A	1550 nm
Dostart et. al. [S11]	2021	Resonator	EO	13.1 dB	18.1 dB	0.18	2 GHz	N/A	1550 nm
Doerr et. al. [S12]	2014	Waveguide	EO	6 dB	4 dB	0.66			
Tzuang et. al. [S13]	2014	Waveguide	EO	2.4 dB	N/A	N/A			
Lira et. al. [S14]	2012	Waveguide	EO	3 dB	70 dB	0.04			
Doerr et. al. [S15]	2011	Waveguide	EO	2 dB	11 dB	0.18			
Yan et. al. [S16]	2020	Resonator	MO	28 dB	1 dB	28			
Yan et. al. [S16]	2020	Waveguide	MO	32 dB	2.3 dB	13.91			
Pintus et. al. [S17]	2019	Waveguide	MO	30 dB	18 dB	1.67			
Zhang et. al. [S18]	2019	Waveguide	MO	30 dB	5 dB	6	1.1 THz †	249.7 GHz †	1550 nm
Zhang et. al. [S18]	2019	Resonator	MO	20 dB	11.5 dB	1.739	1.2 GHz †	N/A†	1550 nm
Du et. al. [S19]	2019	Resonator	MO	40 dB	3 dB	13.3	6.2 GHz †	3.1 GHz†	1520 nm
Bi et. al. [S20]	2019	Resonator	MO	19.5 dB	8 dB	2.6	1.6 GHz	N/A	1520 nm
Huang et. al. [S21]	2017	Resonator	MO	14.4 dB	10 dB	1.44	12.4 GHz †	N/A	1550 nm
Ghosh et. al. [S22]	2012	Waveguide	MO	25 dB	14 dB	1.78	99 GHz †	31 GHz †	1490 nm

- Lowest IL 0.65 dB
- Highest IC/IL FoM ~60 dB/dB
- Outperforms on-chip MO
- No other result near 780 nm

Figure 9. Table extracted from our journal publication [1] that compares previously published chip-scale linear optical isolators (i.e. those without frequency shift) on the important figures of merit. The key isolator figure of merit is the ratio of isolation contrast (IC) to insertion loss (IL). All citations listed can be found in the Supplement of our paper [1]. AO = Acousto-optic, EO = Electro-optic, MO = Magneto-optic.

4.4. Directions for future research efforts

Phase matching and wavelength tuning

The biggest technical challenge in the isolators that we have demonstrated is the phase-matching requirement, as it requires precise alignment of the optical and mechanical modes in momentum-frequency space. This is not easy to achieve and there is a great opportunity for follow-on research on adding fine-tuning controls to the isolator. Specifically, due to fabrication uncertainties it is not easy to predict which optical mode pair will have the correct phase-matching to produce an isolator and makes it difficult to control the operating wavelength. We can consider adding options for both coarse tuning and fine tuning for such an isolator device, where coarse tuning simply involves hopping to a different mode pair. Fine tuning can be implemented easily using electro-optic tuning of the lithium niobate. On the other hand, the course tuning can be implemented by thermal heating which leads to greater refractive index change and hence large wavelength shifts. We illustrate the

mode hopping procedure in Fig. 10. The method relies on the thermo-optic tuning for uniform temperature change ΔT as:

$$\Delta f_{\text{mode}} = 2\pi\omega_0 \frac{dn_{\text{eff}}}{dT} \frac{\Delta T}{n_{\text{g(mode)}}}$$

where $n_{\text{g(mode)}}$ is the distinct group index of each of the resonator mode families. This implies that the TE_{00} and TE_{10} modes will experience different frequency shift, allowing for a mode hop to take place. Fig. 1c presents our experimental results. We demonstrate that we can induce phase-matching of 6 consecutive mode pairs near 780 nm with thermo-optic control, to generate similar isolation performance. A maximum relative tuning of ~ 10 GHz was observed, which was limited by the maximum TEC voltage and the heat retention capability of the system. However, it is possible to realize frequency matching of even more mode pairs with better thermal control. These initial experimental results were presented at the CLEO 2022 conference [4].

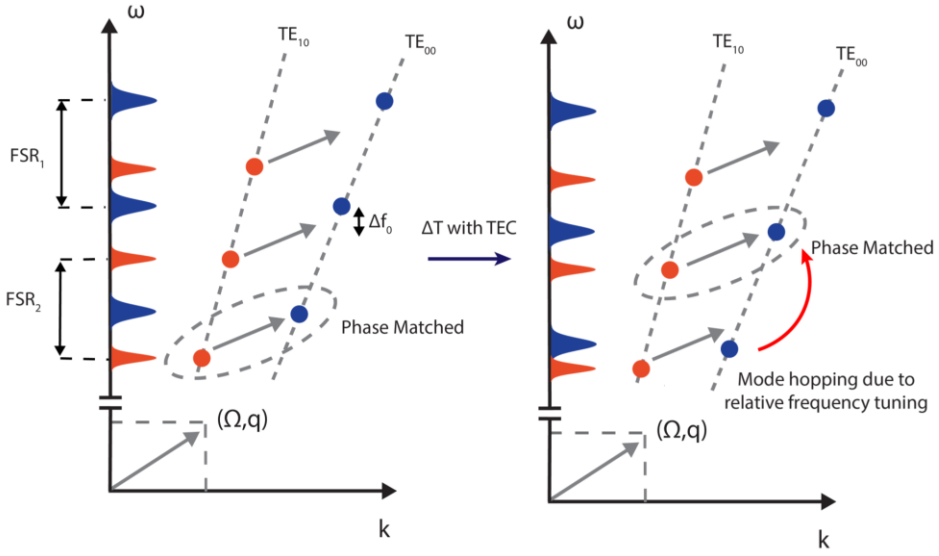

Figure 10. Visualization of the concept of relative tuning of the optical mode families via a thermo-electric cooler (TEC), in order to obtain coarse tuning of the isolator via mode-hopping. Figure reproduced from our conference publication [4].

Improvements needed for practical deployment of this isolator design

For practical deployment, there are a few additional needs that we can identify. First, we need to improve the optical interface, e.g. via fiber-butt coupling and/or inverse tapers, so that the grating coupler loss and reflection is mitigated. There is also an opportunity to demonstrate operation with laser chips through heterogeneous integration. Second, there are numerous tunability and trimming improvements that are needed (as described above) to guarantee device yield such that every device operates as expected or can be trimmed into the operation regime. Third, we need to significantly improve the RF input power efficiency by conducting research on optimizing the optical design, acoustic stimulus design, and RF system design. This latter task may also require a

transition to a different material as the fundamental limits of LN could already have been reached, and as a result this should be considered "DARPA hard".

Adapting the design to new wavelengths of interest to atomic microsystems

As these isolator devices are lithographically patterned in a readily available material, our demonstrated approach could be scaled to cover important wavelengths for atomic metrology – such as 657 nm for Ca atoms and 578 nm for Yb atoms -- with the help of improved designs. Isolators operating at these shorter wavelengths would be very advantageous in atomic microsystems used for sensing and metrology. The challenge with implementing at shorter wavelengths is non-trivial, however, since undesirable scattering caused by surface roughness increases with the 4^{th} power of the frequency. Technically this problem is quite "DARPA hard" and will require unique fabrication solutions and smoothing / annealing operations.

Expanding the isolation bandwidth

The resonant approach that we used in this work provides a very efficient mechanism for producing an optical isolator, but it does come with a bandwidth limitation, i.e. it is restricted to the linewidth of the resonator. A high-impact extension of this work is to develop a non-resonant isolator, e.g. in a waveguide only, that uses either acoustic stimulus (as in this work) or electro-optic stimulus (to be developed) to produce a non-reciprocal transmission effect. This potential effort may require transition to different materials that provide much higher acousto-optic coupling and RF transduction coefficient. Presently, we have already shown preliminary results on non-reciprocal broadband inter-polarization scattering near 780 nm [5].

4.5. Other experimental results and public reporting to the scientific community

In addition to the key journal publication [1], we reported progress on our work through multiple conference presentations and papers [4], [6]–[9]. Some of these intermediate results were developed with aluminum nitride and silicon nitride photonics before we reached the final result with lithium niobate. During the course of this project, we also had the opportunity to explore a dual-resonator design that could simplify some technical aspects of the modulation but cannot yet deliver low insertion loss [10]. All these published experimental results could help direct future research efforts on this topic.

5. Conclusion

Our work can benefit the DARPA and DoD missions by enabling optical isolation for emerging cold-atom technologies in navigation (matter interferometers for gyroscopes), metrology (gravitational, magnetometry), and timekeeping (atomic clocks). Additionally, this work also helps in meeting DARPA's cost and complexity objectives in the context of optical isolation, as it avoids non-standard foundry processes otherwise needed when incorporating magneto-optic materials. As a major feature, electrically driven optomechanical non-reciprocity offers a relatively low-complexity system that can be adapted to any wavelength, in nearly any optical material, and can be extended to many varied DoD applications. More broadly, the technology is also capable of ultralow power optical signal routing and switching, for on-chip photonic systems. This technology also has strong civilian applications in helping make low-cost optical sensors, navigation, and computation systems much more accessible.

References

1 D. B. Sohn, O. E. Örsel, and G. Bahl, "Electrically driven optical isolation through phonon-mediated photonic Autler–Townes splitting," *Nat. Photonics*, vol. 15, no. 11, pp. 822–827, Nov. 2021.

2 D. B. Sohn, S. Kim, and G. Bahl, "Time-reversal symmetry breaking with acoustic pumping of nanophotonic circuits," *Nat. Photonics*, vol. 12, no. 2, pp. 91–97, 2018.

3 D. B. Sohn and G. Bahl, "Direction reconfigurable nonreciprocal acousto-optic modulator on chip," *APL Photonics*, vol. 4, no. 12, p. 126103, Dec. 2019.

4 O. E. Örsel, D. B. Sohn, and G. Bahl, "On-chip lithium niobate isolators at 780 nm with nm-scale tuning bandwidth," in *Conference on Lasers and Electro-Optics*, 2022, p. SW5O.6.

5 O. E. Örsel and G. Bahl, "Electrically-driven Nonreciprocal Polarization Rotation at 780 nm in Thin-Film Lithium Niobate," in *Conference on Lasers and Electro-Optics*, 2022, p. SW5O.7.

6 D. B. Sohn, O. E. Örsel, and G. Bahl, "Low loss wavelength-agnostic optical isolators through acoustic pumping in a lithium niobate platform," in *Frontiers in Optics + Laser Science 2021*, 2021, p. FW1D.4.

7 D. B. Sohn, O. E. Örsel, and G. Bahl, "Electrically-driven linear optical isolation in a lithium niobate nanophotonic platform," in *Conference on Lasers and Electro-Optics*, 2021, p. JTu3A.84.

8 D. B. Sohn, J. Melia, S. Kim, O. E. Orsel, and G. Bahl, "On-chip electrically driven 780 nm frequency-shifting optical isolation," in *Conference on Lasers and Electro-Optics*, 2021, p. STh4B.5.

9 D. Sohn, S. Kim, and G. Bahl, "Unreleased on-chip frequency-shifting optical isolator," in *Conference on Lasers and Electro-Optics*, 2020, p. STh4J.5.

10 S. Kim, D. B. Sohn, C. W. Peterson, and G. Bahl, "On-chip optical non-reciprocity through a synthetic Hall effect for photons," *APL Photonics*, vol. 6, no. 1, p. 011301, Jan. 2021.

LIST OF SYMBOLS, ABBREVIATIONS, AND ACRONYMS

AFRL	Air Force Research Laboratory
AlN	Aluminum Nitride
AO	Acousto-Optic
ATS	Autler-Townes Splitting
CLEO	Conference on Lasers and Electro-Optics
DARPA	Defense Advanced Research Projects Agency
DoD	Department of Defense
EO	Electro-Optic
FoM	Figure of Merit
IC	Isolation Contrast
ICP-RIE	Inductively Coupled Plasma – Reactive Ion Etching
IDT	Interdigitated Transducer
IL	Insertion Loss
LIDAR	Light Detection and Ranging
LN	Lithium Niobate
LNOI	Lithium Niobate on Insulator
MO	Magneto-Optic
PIC	Photonic Integrated Circuit
RF	Radio Frequency
WPAFB	Wright-Patterson Air Force Base